ORIGINAL CONTRIBUTION

Micelle structure of nonionic surfactants containing carbon dioxide moieties in protic ionic liquids

Shurui Miao[1] · Michael Gradzielski[2] · Gregory Warr[1]

Abstract

Partial substitution of ethylene oxide with carbon dioxide moieties can yield greener nonionic surfactants with comparable functionalities. In water, studies showed that the incorporation of CO_2 moieties suppresses the formation of liquid crystalline phases at high concentrations. A similar reduction in solvation and suppression of liquid crystal formation is observed here in the ionic liquids ethylammonium nitrate and propylammonium nitrate. Small-angle neutron scattering is used to study the solvation and packing of micelles in ionic liquids as functions of temperature, concentration, and content of CO_2 moieties. By comparing with aqueous solutions, this work shows that while the nature of surfactant-solvent interaction is comparable among water and alkylammonium nitrate ILs, their behaviours in the solvated micelle shell are different. The lack of liquid crystalline phases should be attributed to the small excluded volume of micelles, which can be fine-tuned via ion design and choice of solvent.

Keywords Self-assembly · Ionic liquids · Carbon dioxide · Neutron scattering

Introduction

Over the past two decades, ionic liquids (ILs) have attracted interest as promising candidates for next-generation solvents. They exhibit negligible vapour pressure and tuneable solvent properties [1–3]. More than 10^6 different ion pairs have been postulated, greatly expanding on the hundreds of organic solvents currently being used in industry and research. Among these, some ILs were found to be inhomogeneous in the bulk [4]. The delicate balance of directional intermolecular interactions (e.g. hydrogen bonding), electrostatic forces, and Van der Waals forces induces molecular segregation resulting in bicontinuous, sponge-like polar/apolar networks in pure ILs [5–7]. This is exemplified by alkylammonium nitrate ILs, among which ethylammonium nitrate (EAN) is the most extensively studied [8]. A series

of structural studies have shown the domain size and correlation length can be controlled through variation of the alkyl length of the cation [1, 8]. The formation of this nanostructure enables them to dissolve a diverse range of polar and apolar solutes, and the presence of this rich pattern of intermolecular forces has made them excellent media for self-assembly [5, 9–12].

The self-assembly of numerous surfactants [10, 13–15] in ILs has been extensively studied, as have other amphiphiles including block copolymers [16–19], biomolecules [20], and even alkanols [9, 21]. Specific counterion effects can complicate studies of ionic surfactants [10, 11, 15, 22–26], making nonionic surfactants preferred solutes to isolate solvation and surfactant packing as functions of IL composition and solvent nanostructure.

Polyoxyethylene n-alkyl ethers (C_nE_m) are the most widely used nonionic surfactants present in almost all cleaning products today. They are often added as polydisperse mixtures (a distribution in headgroup and tail length) to engineer desirable phase behaviour and regulate the viscoelastic properties of the solution. Although among the most widely used surfactants, the ethylene oxide-based headgroups are derived from petrochemicals. This motivated a search for greener replacement, and

✉ Gregory Warr
   gregory.warr@sydney.edu.au

1 School of Chemistry and University of Sydney Nano Institute, The University of Sydney, 2006 Sydney, NSW, Australia

2 Stranski-Laboratorium für Physikalische und Theoretische Chemie, Institut für Chemie, Technische Universität Berlin, Straße des 17. Juni 124, 10623 Berlin, Germany

carbon dioxide stood out as a promising candidate. Recent advances in catalytic processes have enabled large-scale production of nonionic surfactants with CO_2 groups partly substituting ethylene oxide (Fig. 1) [27, 28]. This can be achieved by simply copolymerising ethylene oxide and CO_2 with a suitable catalyst onto the OH-group of a chosen alcohol. These surfactants with CO_2-derived ester groups (CO_2 moieties) can greatly reduce petrochemical consumption and deliver comparable functionalities to conventional nonionic surfactants in aqueous systems [29–32]. More strikingly, the inclusion of even a single CO_2 moiety per surfactant is reported to completely suppress the formation of gel-like liquid crystalline phases in water at high surfactant concentration [29]. This is attributed to reduced headgroup hydration and increasing micelle softness. Ordered packing of these soft micelles is discouraged even at high concentrations, allowing solutions to be much more easily stored and handled, which is of high importance for practical applications.

Previous studies of conventional C_nE_m surfactants in ethylammonium nitrate (EAN) have shown that they can support a wide range of amphiphilic self-assembly behaviour into micelles, lyotropic liquid crystals, and microemulsions [13, 14, 33, 34]. Systematic trends in micelle morphology and phase behaviour are observed parallel to their aqueous analogues [14]. In this study, we have investigated micelle formation by nonionic surfactants containing CO_2 moieties in two ionic liquids, EAN and propylammonium nitrate (PAN). We used small-angle neutron scattering (SANS) to elucidate how this modification of the headgroup influences its interaction with IL solvents and thereby modulates their aggregation properties. Dodecyl and hexadecyl surfactants with varying CO_2 moiety contents are studied at multiple temperatures and compositions, allowing us to also assess the effect of the alkyl chain length on the aggregation behaviour. The aim of this investigation was to provide insight into the origin of solvophobicity displayed in ILs [35], the interaction between ILs and the modified surfactant headgroups, and to compare this behaviour to that previously observed in water. This will enable rational design of phase behaviours via choice of solvents.
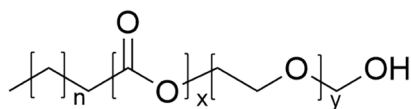
Fig. 1 Structure of nonionic surfactant with CO_2-derived ester groups, $C_{n+2}(E)_y(CO_2)_xOH$, $n=10$ or 14. The headgroup is a statistical copolymer of ethylene oxide and carbon dioxide. Average headgroup compositions and molecular masses are shown in Table 1. Mass spectra are shown in Fig. S1

Materials

Octaethylene glycol monohexadecyl ether ($C_{16}E_8$) was purchased from Nikkol and used as received. Other surfactants containing CO_2 moieties (Table 1) were developed and produced by Covestro via copolymerisation of ethylene oxide with CO_2 applying an alkyl alcohol as the initiator and a bimetallic catalyst. Electrospray mass spectrometry was employed to verify their alkyl length and headgroup size (see SI). All samples were stored in a freezer at $-20\ °C$, and the average molecular mass is given in Table 1.

Partially deuterated d_3-ethylammonium nitrate (EAN) and d_3-propylammonium nitrate (PAN) were prepared by neutralisation of nitric acid with the corresponding alkylamine, followed by deuteration of exchangeable hydrogens. Ethylamine solution (66–72%, Sigma), propylamine (99%, Sigma), and nitric acid (70%, Ajax) were used as received. Amine solutions were diluted in water to ~20 wt% before being added dropwise to the diluted nitric acid solution (~20 wt%). The mixture was under constant stirring and kept in an ice bath. Temperature was maintained below 10 °C and the titration is conducted until pH indicated the reaction mixture was in slight excess of amine. Bulk water was removed using a rotary evaporator (30 mbar, 40 °C). Deuteration of exchangeable protons was performed by adding 3:1 mol/mol D_2O to ILs. Bulk water was removed by rotary evaporation, and exchange was repeated 5 times per IL sample. Trace water was removed under a high vacuum over > 48 h (0.2 mbar, room temperature). Final water content is < 0.2 wt% (Karl Fischer titration), and 300 MHz ^1H NMR confirmed that all exchangeable protons had been replaced by deuterium.

Methods

Diffusive interfacial transport experiments were performed to confirm the absence of liquid crystalline phases [36, 37]. A Leica DM 2500p microscope fitted with a polariser was used. Here, a drop of molten dry surfactant is added to a

Table 1 Average compositions and molecular masses of nonionic surfactants used in this study. C16E8 is monodisperse but all other samples are industrial mixtures of various headgroup sizes, and the averaged value is used

Surfactant	M_n (g/mol)	Abbreviation
$C_{12}(EO)_{8.2}(CO_2)_{3.1}OH$	680.21	C12E8C3
$C_{16}(EO)_8OH$	594.86	C16E8
$C_{16}(EO)_{9.3}(CO_2)_{1.5}OH$	707.09	C16E9C2
$C_{16}(EO)_{7.8}(CO_2)_{2.8}OH$	708.64	C16E8C3
$C_{16}(EO)_{14.6}OH$	824.97	C16E15

clean glass slide and covered by a thin coverslip. A drop of solvent is added to the corner of the coverslip. Due to the capillary effect, the solvent is drawn into the gap between the coverslip and glass slide. As the solvent meets the surfactant, a continuous concentration gradient is created between pure solvent and pure surfactant. This enables all phases that exist at any composition at the specified temperature to be generated. Crossed polarisers are used to help identify liquid crystalline phases that display birefringence. Images were captured using a QImaging MicroPublisher 3.3 RTV camera with 200 times magnification.

Small-angle neutron scattering (SANS) measurements were performed on the *Quokka* beamline at the Australian Centre for Neutron Scattering with hydrogenous surfactants in partially deuterated ILs (single contrast). Neutrons with average wavelengths of 5.0 and 6.0 Å and a $\Delta\lambda/\lambda$ up to 15% were selected with a velocity selector. Scattering was collected from 1.0-mm path length samples at two sample-to-detector distances of 4 and 14 m, giving a combined range of $0.004 < q < 0.4$ Å^{-1}. Acquisition was performed at 308, 343, and 378 K. Isotropic scattering patterns collected on a 2D detector were reduced to I(q) using modified NIST routines in Igor™.

Model fits to the SANS patterns are shown and described in the SI. In order to facilitate comparison with these systems in water, we have followed the analysis described previously. Forward scattering intensities, *I(0)*, were used to extract the structure factor at the thermodynamic limit (*S(0)*) in the monodisperse approximation (Eq. 1) [29].

$$I(0) = \phi_{\mathrm{dry}} \cdot \Delta\rho^2 \cdot V \cdot S(0) \tag{1}$$

where ϕ_{dry} is the dry volume fraction of surfactant calculated from theoretical aggregation number and it is in good agreement with published density of conventional nonionic surfactants (see SI) [38], $\Delta\rho$ is the difference in scattering length densities of dry micelles and solvent, and *V* is the volume of the dry micelle. For the model of hard-spheres,

S(0) is accurately described by the Carnahan-Starling model (Eq. 2) [39].

$$S(0)^{-1} = \frac{\left(1 + 2\phi_{\mathrm{hs}}\right)^2 - 4\phi_{\mathrm{hs}}^3 + 4\phi_{\mathrm{hs}}^4}{\left(1 - \phi_{\mathrm{hs}}\right)^4} \tag{2}$$

This model was then used to determine the effective, concentration-dependent, hard-sphere volume fraction (ϕ_{hs}) of the dispersed micelles according to Eq. (2). The relationship between measured ϕ_{hs} and the actual volume fraction of surfactant added, ϕ_{dry}, is modelled by Eq. (3) [29].

$$\phi_{\mathrm{hs}} = B\phi_{\mathrm{dry}}(1 - A\phi_{\mathrm{dry}}) \tag{3}$$

Both *B* and *A* are parameters that describe two different concentration-dependent effects regarding the effective volume of the micelles. *B* accounts for the solvation of dry micelles which increases their effective volume fraction, i.e. the volume ratio of solvated to dry micelles (which must be > 1). The parameter *A* accounts for the interpenetration of neighbouring micelles which occurs with increasing micelle concentration and reduces the effective volume fraction [29]. *A* is a second-order term and therefore negligible at low concentrations, but being quadratic in the volume fraction becomes increasingly dominant at higher concentrations. In molecular terms, $A\phi_{\mathrm{dry}}$ can be interpreted as the fraction of the initial hard-sphere volume (present at infinite dilution, $B\phi_{\mathrm{dry}}$) that becomes penetrable at a finite concentration.

Results and discussion

Figure 2 shows diffusive interfacial transport images of polydisperse C16E15 (Fig. 2A) and C16E8C3 (Fig. 2B) in EAN at 296 K. Neither surfactant forms birefringent liquid crystalline phases, but the deformed air bubble near the solid–liquid interface of C16E15 (Fig. 2A) is diagnostic for an isotropic, gel-like cubic phase. In contrast, the

Fig. 2 Polarised microscopy images of diffusive interfacial transport experiments at 296 K for **A** C16E15 and **B** C16E8C3 in EAN. The top right corner is pure surfactant and solvent is added from the bottom left corner of each image
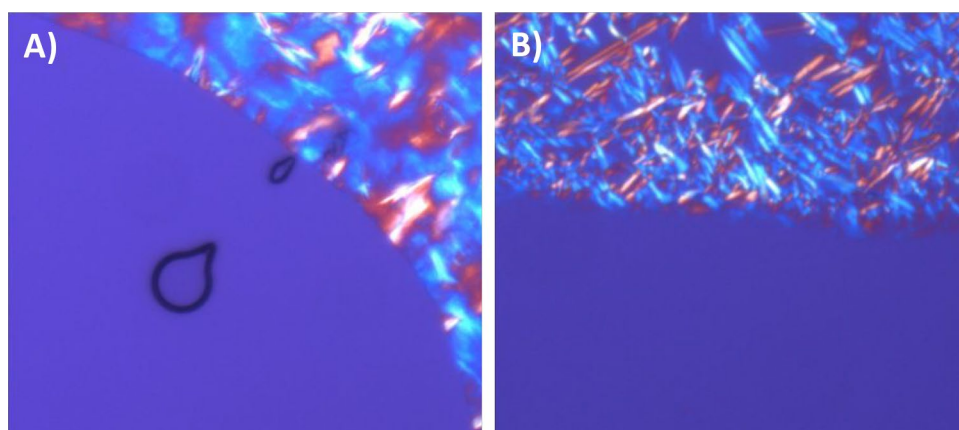
solid–liquid interface of C16E8C3 with EAN displayed a smooth boundary from which any trapped bubbles could easily diffuse away indicating that no cubic phase occurs in C16E8C3-EAN mixtures at any compositions. This is consistent with existing literature in water, where the incorporation of CO_2 moieties can completely suppress the formation of liquid crystalline phases [29]. To understand the origin of this behaviour and the interaction between micelles, SANS experiments were performed.

Figure 3 shows representative SANS patterns of selected surfactants in EAN at 308 K, above the Krafft temperature of the hexadecyl surfactants. Figure 3A shows the results found for all surfactants at 5 wt% and 308 K (complete dataset of all compositions and temperatures are shown in Figs. S2−S5), which is consistent with the formation of spherical core–shell micelles above a critical micelle concentration (CMC). Figure 3B shows that with increasing concentration, scattered intensity increases, and an interaction peak (structure factor) develops above 5 wt%. The upturn in intensity at $q < 0.01$ Å^{-1}, which is most apparent in C12E8C3, due to the low scattering intensity from the sample, is likely due to microbubbles trapped within the sample cell [14].
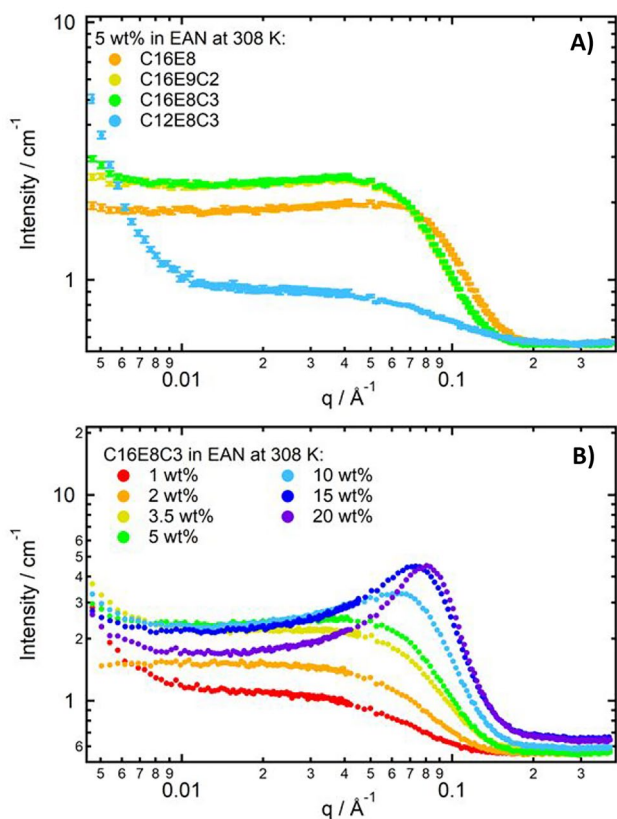
Fig. 3 Representative SANS patterns of nonionic surfactants in EAN at 308 K. **A** 5 wt% solutions of C16E8, C16E9C2, C16E8C3, and C12E8C3 and **B** all concentrations of C16E8C3

Table 2 Critical micelle concentrations (CMCs) in EAN and PAN estimated using invariant analysis. The CMC of C12E8C3 in PAN could not be determined as micelles were only observed in one sample above 10 wt%. Details are provided in SI

Surfactant	CMCs (wt%)	
	EAN	PAN
C12E8C3	2.0 ± 1.7	> 10
C16E8C3	0.70 ± 0.56	1.2 ± 0.7
C16E9C2	0.79 ± 0.70	1.4 ± 0.4
C16E8	0.72 ± 0.48	2.6 ± 0.8

The scattering patterns of C16E9C2 and C16E8C3 at 5 wt% (Fig. 3A) are almost identical, suggesting that the formation of micelles is insensitive to small differences in the extent of CO_2 incorporation. However, both C16 surfactants containing CO_2 moieties show a higher scattering intensity, and the intensity upturn occurs at a lower q than that of C16E8 (near 0.1 Å^{-1}), both indicating that surfactants with CO_2 moieties form larger micelles. We also noticed that for the most highly concentrated samples, the correlation peak is much sharper for C16E8 than C16 surfactants containing CO_2 moieties (e.g. Fig. S2). This indicates that the repulsions between micelles at the same concentration are stronger in C16E8 than surfactant containing CO_2 moieties, similar to their behaviour in water [31].

The lower overall scattering intensity of the C12E8C3 solution is due to its much higher CMC. This is clear from the absence of C12E8C3 micelles in EAN below 2 wt% (Fig. S2), and from invariant analysis (see Fig. S7), which yields the CMC values listed in Table 2. Similar dependence of CMC on alkyl chain length is reported in water and EAN [14].

CMCs are much higher in PAN than EAN, which is higher than in water (e.g. C12E8C3 is 0.0036 wt%, $C16E_xC_y$ CMCs in water are not available due to poor solubility) [29]. C12E8C3 can no longer form well-defined micelles up to 10 wt%, indicating that the minimum alkyl chain length required to stabilise micelles is greater in PAN than in EAN, as also seen in conventional polyoxyethylene surfactants [34]. Similarly, no micelles were observed by SANS in C16 surfactants up to 2 wt% in PAN, and 5 wt% solutions yielded lower-than-expected total coherent scattering and volume fraction, both consistent with elevated CMC.

Fitting of the SANS data to a core–shell sphere form factor with hard-sphere structure factor did not yield a unique and consistent set of physically meaningful fits [14, 31]. This is likely due to interpenetration of the headgroups, as was found for these systems in aqueous solution (see SI for details).

To further explore the intermicellar interactions and facilitate comparison with aqueous solutions, we instead analysed the forward scattering, $I(0)$, in terms of effective volume
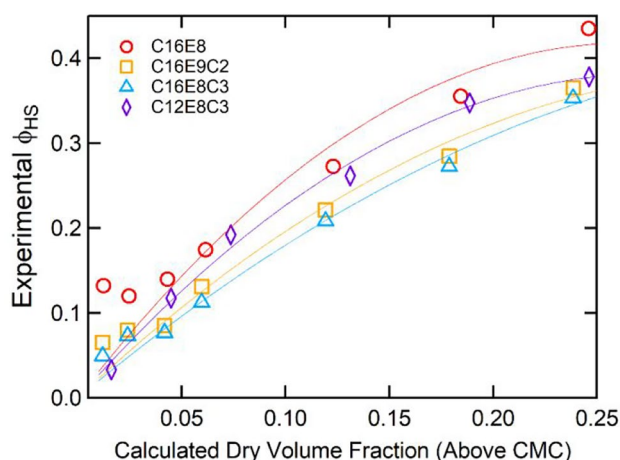
Fig. 4 Variation of experimental hard-sphere volume fraction, ϕ_{hs}, of surfactant solutions from SANS data with dry volume fraction, ϕ_{dry}, corrected by its CMC. Lines show the best fit to Eq. (3)

fraction for a hard-sphere interaction as outlined in the "Methods" Section [29]. All scattering curves exhibit plateaus at $q < 0.02$ Å^{-1} (see Fig. 3 and Figs. S2–S6), enabling the thermodynamic limit, $I(0)$, to be determined. $I(0)$ first increases with increasing concentration as more micelles are present, and the total scattering volume increases and then decreases as the packing of micelles becomes increasingly ordered. This structure factor effect leads to the development of a peak near 0.05 Å^{-1}, which becomes more pronounced and shifts to higher q with increasing surfactant concentration as the average separation between micelles decreases.

Fits to Eq. (3) and the derived fit parameters are shown in Fig. 4 and Table 3, respectively, assuming that the micelle aggregation number is independent of concentration [14]. Good fits are obtained overall, especially at high surfactant concentrations. The dry micelle volume fraction for C12E8C3 has been corrected for its CMC of 2.5 wt% but

Table 3 Micelle solvation, B, and softness, A, determined from fits to Eq. (3), represented as multiples of dry micelle volume. Solvent per surfactant is calculated based on the known solvent density and micelle aggregation number (see SI for details). Values for aqueous solutions are taken from ref [29].

Surfactant-solvent	Solvation, B	Softness, A	Solvent per surfactant
C12E8C3-EAN	2.8	1.8	12.8
C16E8C3-EAN	2.1	1.2	8.3
C16E9C2-EAN	2.3	1.5	10.2
C16E8-EAN	3.2	1.9	14.7
C12E8C3-water	1.51	0.55	17.2
C12E12C2-water	1.58	0.52	19.7
C12E11C1-water	1.63	0.50	23.2
C12E13-C1-water	1.64	0.37	25.2
C12E14-water	1.72	0.01	28.8

neglected for C16 surfactant which may explain the slight discrepancies observed for the lowest concentrations (see SI). This is most pronounced for C16E8, which has a higher CMC than the other two C16 surfactants as shown by the relatively low scattering intensity in Fig. 3A. Nevertheless, this has negligible impact to the fit over the entire concentration range, and the subtle differences in CMCs among C16 surfactants are negligible within the uncertainties of the invariant analysis (Table 2).

Table 3 shows that all four surfactant systems yielded a solvation value, B, greater than two in EAN. This means that isolated micelles in dilute solution occupy more than twice their dry volume due to solvation, which are significantly larger than the corresponding values (for C12 surfactants with same headgroups) in water. This means the headgroup layer of the micelles is much more swollen and the headgroups themselves protrude further into their surroundings in EAN. The solvation numbers of each surfactant are smaller, however, as the volume of each EAN ion pair is much larger than a single water molecule [29].

The hydration of C12E14 of 28.8 corresponds well to approximately two water molecules per ether oxygen hydrogen bonding acceptor [41]. In EAN, the ethylammonium cation can donate into three H-bonds, from which the predicted IL/surfactant ratio should be around 0.67 that of water. This is consistent with our results of 17.2 water molecules versus 12.8 EAN per C12E8C3 [29] and suggests that the solvophilic solvent-headgroup interaction of nonionic surfactants with alkylammonium ILs is also governed by hydrogen bonding.

Increasing alkyl length to C16E8C3 reduces the EAN/surfactant ratio. This is likely due to the formation of larger micelles reducing the curvature of the headgroup shell, so that less volume is available per surfactant to be occupied by solvent species. Despite having the smallest headgroup, C16E8 has the largest solvation in EAN, confirming that the incorporation of CO_2 moieties reduces headgroup solvation in EAN, just as it does in aqueous systems [29].

The main difference to the aqueous system is that the softness parameter A does not increase with increasing content of CO_2 moieties but slightly decreases. This means the pure ethylene oxide headgroup shows a high degree of interpenetration in EAN. This difference may be attributed to the large volume of micelles in EAN (i.e. the B parameter in EAN is substantially bigger than in water). More swollen micelles means the micellar shell is more prone to penetration. Furthermore, water is a stronger H-bond donor relative to the less polar N–H bonds in ethylammonium cations and therefore is more tightly H-bonded to the ethylene oxide groups. In a similar direction, the difference between B and A is 1.7 and 1.3 (Table 3) in water and EAN, respectively [14, 29], which means that the relative effect of the interpenetration

of shells (softness) is more pronounced in EAN compared to water.

The solvophobic interaction that gives rise to amphiphilic nanostructure in EAN itself has been shown to also cause ethylammonium ions to associate with surfactant aggregates [15]. The IL cation can preferentially orient at apolar interfaces and exhibit co-surfactant-like behaviour by embedding its alkyl tail into the micelle core. These amphiphilic IL cations may slightly swell the micelle cores, also contributing to softer micelles overall.

With increasing temperature, the SANS patterns of all surfactants in both EAN and PAN exhibit less sharp correlation peaks, the peaks are shifted to lower q, and the overall scattering intensity increases. These changes indicate a growth of the micelles with rising temperature and possible increase in polydispersity. SANS patterns of surfactants containing CO_2 moieties in ILs at elevated temperature can no longer be modelled by interacting spheres, requiring the core to become ellipsoidal (see SI) [32]. This transition is also consistent with past studies of polyoxyethylene surfactants in water and EAN. In both solvents, micelle growth occurs as the temperature approaches their cloud point [14, 42–44] and confirms that the thermal response of these surfactants is comparable to conventional nonionic surfactants. This is attributed to the reduced solvation with increasing temperature, thereby reducing the effective headgroup area and surfactant packing. The scattering patterns of the PAN samples (Fig. S6) show that this increase of scattering intensity with temperature is more pronounced for pure C16E8 than surfactants containing CO_2 moieties, where most likely an increasing CMC leads to demicellisation.

In water, EAN, and PAN, the minimum alkyl chain length for conventional nonionic surfactants to form well-defined micelles at low concentrations (i.e. low CMC) is C10, C14, and C16, respectively [14, 34, 41]. Our results confirm that a similar trend applies to nonionic surfactants with CO_2 moieties, indicating that the driving force of self-assembly is largely unaffected by headgroup modification [40]. From the CMC values, we can conclude that the free energy of micellisation, $\Delta G°_{mic}$, of hexadecyl surfactants in PAN is lower than in EAN by about a kT, which is itself 6 kT smaller than in water.

Conclusion

The incorporation of CO_2 moieties in the headgroup of nonionic surfactants has a negligible effect on the tendency to form micelles. The solvophobic driving force for self-assembly is governed by the alkyl chain length of surfactant and the average polarity and nanostructure of the solvent. However, the presence of CO_2-derived

ester groups in the headgroup can modulate the solvent-headgroup interaction. Higher content of CO_2 moieties is observed to suppress solvent-headgroup hydrogen bonding which reduces solvation in ILs as it does in water.

While the underlying molecular interaction is similar, this has led to different trends in micelle softness in water and EAN. In water, the micelle softness increases (or the extent of interpenetration among nearest micelles, captured by parameter A) with content of CO_2 moieties. This is attributed to the reduced hydration of the micellar headgroup [29]. In contrast, micelles in EAN are inherently more swollen due to the larger EAN molar volume (relative to water), and micelles become less penetrable with increasing content of CO_2 moieties, opposite to water. Alkylammonium IL cations can act as a co-surfactant and undergo dynamic exchange between the solvation and bulk state [15, 45–47]. As a result, the relatively large volume of ILs in micellar shell can become easily displaced by chain-chain interpenetration among neighbouring micelles. This allows well-solvated micelles to be softer than poorly solvated ones in ILs.

Overall, the effect of incorporation of CO_2 moieties into nonionic surfactant headgroups has the same effect of decreasing solvation in ILs and in water. The co-surfactant behaviour of ILs has induced a different trend in the ability to interpenetrate among neighbouring micelles as the content of CO_2 moieties increases. Nevertheless, the excluded volume per micelle in ILs for surfactants containing CO_2 moieties is comparable to, if not lower than, that of water. This suppresses the formation of liquid crystalline phases, allowing concentrated solutions to be easily handled as low-viscosity fluids. Differences in H-bonding and amphiphilic character of water and EAN highlight that solvent can be used as a tool to fine-tune micelle properties and inter-micelle interactions.

Data Availability The authors declare that the data supporting the findings of this study are available within the paper and its Supplementary Information files. Should any raw data files be needed in another format they are available from the corresponding author upon reasonable request.

Declarations

Conflict of interest The authors declare no competing interests.

References

1. Hayes R, Imberti S, Warr GG, Atkin R (2014) Effect of cation alkyl chain length and anion type on protic ionic liquid nanostructure. J Phys Chem C 118:13998–14008

2. Greaves TL, Kennedy DF, Mudie ST, Drummond CJ (2010) Diversity observed in the nanostructure of protic ionic liquids. J Phys Chem B 114:10022–10031

3. Greaves TL, Weerawardena A, Fong C, Krodkiewska I, Drummond CJ (2006) Protic ionic liquids: solvents with tunable phase behavior and physicochemical properties. J Phys Chem B 110:22479–22487

4. Hayes R, Warr GG, Atkin R (2015) Structure and Nanostructure in ionic liquids. Chem Rev 115:6357–6426. https://doi.org/10.1021/cr500411q

5. Greaves TL, Drummond CJ (2008) Ionic liquids as amphiphile self-assembly media. Chem Soc Rev 37:1709–1726. https://doi.org/10.1039/b801395k

6. Greaves TL, Weerawardena A, Fong C, Drummond CJ (2007) Many protic ionic liquids mediate hydrocarbon-solvent interactions and promote amphiphile self-assembly. Langmuir 23:402–404

7. Greaves TL, Drummond CJ (2013) Solvent nanostructure, the solvophobic effect and amphiphile self-assembly in ionic liquids. Chem Soc Rev 42:1096–1120

8. Hayes R, Imberti S, Warr GG, Atkin R (2011) Amphiphilicity determines nanostructure in protic ionic liquids. Phys Chem Chem Phys 13:3237–3247. https://doi.org/10.1039/C0CP01137A

9. Jiang HJ, FitzGerald PA, Dolan A, Atkin R, Warr GG (2014) Amphiphilic self-assembly of alkanols in protic ionic liquids. J Phys Chem B 118:9983–9990. https://doi.org/10.1021/jp504998t

10. Bryant SJ, Atkin R, Gradzielski M, Warr GG (2020) Catanionic surfactant self-assembly in protic ionic liquids. J Phys Chem Lett 11:5926–5931. https://doi.org/10.1021/acs.jpclett.0c01608

11. Dolan A, Atkin R, Warr GG (2015) The origin of surfactant amphiphilicity and self-assembly in protic ionic liquids. Chem Sci 6:6189–6198. https://doi.org/10.1039/c5sc01202c

12. Fernández-Castro B et al (2011) Surfactant self-assembly nanostructures in protic ionic liquids. J Phys Chem B 115:8145–8154. https://doi.org/10.1021/jp203204c

13. Araos MU, Warr GG (2005) Self-assembly of nonionic surfactants into lyotropic liquid crystals in ethylammonium nitrate, a room-temperature ionic liquid. J Phys Chem B 109:14275–14277

14. Araos MU, Warr GG (2008) Structure of nonionic surfactant micelles in the ionic liquid ethylammonium nitrate. Langmuir 24:9354–9360

15. Lam MT, Adamson WD, Miao S, Atkin R, Warr GG (2019) DTAB micelle formation in ionic liquid/water mixtures is determined by ionic liquid cation structure. J Colloid Interface Sci 552:597–603. https://doi.org/10.1016/j.jcis.2019.05.082

16. López-Barrón CR, Li D, DeRita L, Basavaraj MG, Wagner NJ (2012) Spontaneous thermoreversible formation of cationic vesicles in a protic ionic liquid. J Am Chem Soc 134:20728–20732. https://doi.org/10.1021/ja308975e

17. Zhang G et al (2008) Lyotropic liquid-crystalline phases formed by Pluronic P123 in ethylammonium nitrate. J Phys Chem B 112:6578–6584. https://doi.org/10.1021/jp800130p

18. Jain NJ, Aswal VK, Goyal PS, Bahadur P (1998) Micellar structure of an ethylene oxide propylene oxide block copolymer: a small-angle neutron scattering study. J Phys Chem B 102:8452–8458. https://doi.org/10.1021/jp982568o

19. Atkin R, De Fina LM, Kiederling U, Warr GG (2009) Structure and self assembly of pluronic amphiphiles in ethylammonium nitrate and at the silica surface. J Phys Chem B 113:12201–12213. https://doi.org/10.1021/jp9063627

20. Bryant SJ, Wood K, Atkin R, Warr GG (2017) Effect of protic ionic liquid nanostructure on phospholipid vesicle formation. Soft Matter 13:1364–1370. https://doi.org/10.1039/C6SM02652D

21. Miao S, Imberti S, Atkin R, Warr G (2022) Nanostructure in amino acid ionic molecular hybrid solvents. J Mol Liq 351:118599. https://doi.org/10.1016/j.molliq.2022.118599

22. Sanchez-Fernandez A et al (2018) Counterion binding alters surfactant self-assembly in deep eutectic solvents. Phys Chemi Chem Phys 20:13952–13961. https://doi.org/10.1039/C8CP01008K

23. Sanchez-Fernandez A, Jackson AJ, Prévost SF, Doutch JJ, Edler KJ (2021) Long-range electrostatic colloidal interactions and specific ion effects in deep eutectic solvents. J Am Chem Soc 143:14158–14168. https://doi.org/10.1021/jacs.1c04781

24. Lee AA, Perez-Martinez CS, Smith AM, Perkin S (2017) Scaling analysis of the screening length in concentrated electrolytes. Phys Rev Lett 119:5. https://doi.org/10.1103/PhysRevLett.119.026002

25. Gebbie MA et al (2013) Ionic liquids behave as dilute electrolyte solutions. Proc Natl Acad Sci 110:9674. https://doi.org/10.1073/pnas.1307871110

26. Lee AA, Vella D, Perkin S, Goriely A (2015) Are room-temperature ionic liquids dilute electrolytes? J Phys Chem Lett 6:159–163. https://doi.org/10.1021/jz502250z

27. Poland SJ, Darensbourg DJ (2017) A quest for polycarbonates provided via sustainable epoxide/CO_2 copolymerization processes. Green Chem 19;4990–5011. https://doi.org/10.1039/C7GC02560B

28. Grignard B, Gennen S, Jérôme C, Kleij AW, Detrembleur C (2019) Advances in the use of CO_2 as a renewable feedstock for the synthesis of polymers. Chem Soc Rev 48:4466–4514. https://doi.org/10.1039/C9CS00047J

29. Spiering VJ et al (2020) Changes in Phase behavior from the substitution of ethylene oxide with carbon dioxide in the head group of nonionic surfactants. ChemSusChem 13:601–607. https://doi.org/10.1002/cssc.201902855

30. Lima MT et al (2019) The hydrophilic-lipophilic balance of carboxylate and carbonate modified nonionic surfactants. Colloids Surf A Physicochem Eng Asp 569:156–163. https://doi.org/10.1016/j.colsurfa.2019.03.001

31. Spiering VJ, Lutzki J, Gradzielski M (2021) Thermodynamics of micellization of nonionic surfactants - the effect of incorporating CO_2 moieties into the head group. J Colloid Interface Sci 581:794–805. https://doi.org/10.1016/j.jcis.2020.07.141

32. Spiering VJ, Prause A, Noirez L, Appavou M-S, Gradzielski M (2021) structural characterization of nonionic surfactant micelles with CO$_2$/ethylene oxide head groups and their temperature dependence. Langmuir 37:13235–13243. https://doi.org/10.1021/acs.langmuir.1c01737

33. Atkin R, Warr GG (2007) Phase behavior and microstructure of microemulsions with a room-temperature ionic liquid as the polar phase. J Phys Chem B 111:9309–9316

34. Atkin R, Bobillier SMC, Warr GG (2010) Propylammonium nitrate as a solvent for amphiphile self-assembly into micelles, lyotropic liquid crystals, and microemulsions. J Phys Chem B 114:1350–1360

35. Marlow JB, Atkin R, Warr GG (2023) How does nanostructure in ionic liquids and hybrid solvents affect surfactant self-assembly? J Phys Chem B 127:1490–1498. https://doi.org/10.1021/acs.jpcb.2c07458

36. Laughlin RG (1994) The aqueous phase behaviour of surfactants. 1st edn, (ACADEMIC PRESS)

37. Laughlin RG, Munyon RL (1987) Diffusive interfacial transport: a new approach to phase studies. J Phys Chem 91:3299–3305. https://doi.org/10.1021/j100296a038

38. Berthod A, Tomer S, Dorsey JG (2001) Polyoxyethylene alkyl ether nonionic surfactants: physicochemical properties and use for cholesterol determination in food. Talanta 55:69–83. https://doi.org/10.1016/S0039-9140(01)00395-2

39. Carnahan NF, Starling KE (1969) Equation of state for nonattracting rigid spheres. J Chem Phys 51:635–636. https://doi.org/10.1063/1.1672048

40. Shi L, Zheng L (2012) Aggregation behavior of surface active imidazolium ionic liquids in ethylammonium nitrate: effect of alkyl chain length, cations, and counterions. J Phys Chem B 116:2162–2172. https://doi.org/10.1021/jp211338k

41. Mitchell DJ, Tiddy GJT, Waring L, Bostock T, McDonald MP (1983) Phase behaviour of polyoxyethylene surfactants with water. Mesophase structures and partial miscibility (cloud points). J Chem Soc Faraday Trans II 79:975–1000.

42. Israelachvili JN, Mitchell DJ, Ninham BW (1976) Theory of self-assembly of hydrocarbon amphiphiles into micelles and bilayers. J Chem Soc Faraday Trans II(72):1526–1568

43. Tlusty T, Safran SA, Menes R, Strey R (1997) Scaling laws for microemulsion governed by spontaneous curvature. Phys Rev Letters 78:2616–2619

44. Blom A, Warr GG, Wanless EJ (2005) Morphology transitions in nonionic surfactant adsorbed layers near their cloud points. Langmuir 21:11850–11855. https://doi.org/10.1021/la0520334

45. Miao S, Hoffmann I, Gradzielski M, Warr GG (2022) Lipid membrane flexibility in protic ionic liquids. J Phys Chem Lett 13:5240–5245. https://doi.org/10.1021/acs.jpclett.2c00980

46. Murphy T, Hayes R, Imberti S, Warr GG, Atkin R (2016) Ionic liquid nanostructure enables alcohol self assembly. Phys Chem Chemi Phys 18:12797–12809. https://doi.org/10.1039/c6cp01739h

47. Stetter FWS, Hugel T (2013) The nanomechanical properties of lipid membranes are significantly influenced by the presence of ethanol. Biophys J 104:1049–1055. https://doi.org/10.1016/j.bpj.2013.01.021